Lateral Flow Assays Biotesting by Utilizing Plasmonic Nanocrystals Made of Inexpensive Metals – Replacing Gold

Veronica A. Bahamondes Lorca[1,2], Oscar Ávalos-Ovando[3,4], Christoph Sikeler[5], Eva Yazmin Santiago[3,4], Eli Skelton[4,6], Yong Wang[7], Ruiqi Yang[7], Katherine Leslee A. Cimatu[4,6], Olga Baturina[8], Zhewei Wang[9], Jundong Liu[9], Joseph M. Slocik[10], Shiyong Wu[1,6], Dongling Ma[7], Andrei I. Pastukhov[11], Andrei Kabashin[11], Martin E. Kordesch[3,4], and Alexander O. Govorov[3,4*]

[1] Edison Biotechnology Institute, Ohio University, Athens, Ohio 45701, United States

[2] Departamento de Tecnología médica, Facultad de Medicina, Universidad de Chile, Santiago, Chile

[3] Department of Physics and Astronomy, Ohio University, Athens, Ohio 45701, United States

[4] Nanoscale and Quantum Phenomena Institute, Ohio University, Athens, Ohio 45701, United States

[5] Faculty of Physics and Center for NanoScience (CeNS), Ludwig Maximilians University, 80539 Munich, Germany

[6] Department of Chemistry and Biochemistry, Ohio University, Athens, Ohio 45701, United States

[7] Institut National de la Recherche Scientifique,Varennes, Québec J3X 1P7, Canada

[8] Chemistry Division, United States Naval Research Laboratory, Washington DC 20375, United States

[9] School of Electrical Engineering and Computer Science, Ohio University, Athens, Ohio 45701, United States

[10] Soft Matter Materials Branch, Materials and Manufacturing Directorate, Air Force Research Laboratory, Wright Patterson Air Force Base, Ohio 45433-7750, United States

[11] Laboratory LP3, Campus de Luminy, Aix-Marseille University, CNRS, 13288 Marseille, France

* Corresponding authors: govorov@ohio.edu

Keywords: optical activity, nanoparticles, lateral flow assay, biomarkers.

Abstract

Different kinds of nanoparticles can be conjugated with diverse biomolecular receptors and employed in biosensing to detect a target analyte (biomarkers of infections, cancer markers, etc.) from biological samples. This proven concept was largely used during the COVID-19 pandemic in over-the-counter gold nanoparticles-based paper strip tests. Considering that gold is expensive and is being largely depleted, here we show that novel and less expensive plasmonic counterparts, titanium nitride (TiN) nanoparticles, and copper nanoparticles covered with a gold shell (Cu@Au) perform comparable or better than gold nanoparticles. After functionalization, these novel nanoparticles provide a high signal, efficiency, and specificity when used on paper strip tests. This allows an easy visual determination of the positive signal and the development of more affordable paper-based test strips. Moreover, by conducting the machine learning study, we have shown that the bio-detection with TiN is more accurate than that with gold, demonstrating the advantage of a broadband plasmonic material. The implementation of lateral flow assays based on TiN and Cu@Au nanoparticles promises a drastic cost reduction of this technology and its widespread applications in tasks of biomedical diagnostics, environmental and food safety, security and doping screening.

The recent worldwide pandemic taught us that we were not fully prepared to undergo immediate massive and cheap preventive testing, which at the same time needed to be reliable and easy to use. Nanotechnology and nanomaterials provide great opportunities for technological development in diverse areas. From a medical point of view, nanotechnology and nanomaterials represent a still fully undiscovered frontier of novel potential uses applicable to advanced medical treatments, both for diagnostics and therapy. At the heart of all this technology are plasmonic

nanoparticles (NPs), generally gold NPs (Au NPs) [1]. Surface chemistry flexibility allows the binding of diverse molecules to the NP's surface, acting the NP as a vehicle for biomolecules such as antibodies [2] and allowing the NPs to play a significant role in nanophotonic biosensing [3, 4].

Additional to the already established Au NPs-based Covid-19 tests market [5-7], there is also a vast market of colorimetric testing systems for other various important biomarkers and biomolecules, regularly commercialized in the so-called lateral-flow assays (LFAs) [8-10]. LFAs are inexpensive and quick, and, for the most part offer a reliable way of analyzing diverse biomarkers in either home or point of care testing, in diverse situations such as pregnancy tests, diabetes markers, and strokes controls, among many others (see Fig. 1A). Hence, LFAs should provide the ideal testing platform for large-scale distributions to face eventual new pandemics or for controlling regular illnesses with everyday testing. As such, recent significative studies have focused on improving LFAs. For example, SARS-CoV-2 antibody-conjugated fluorescent gold nanorods were recently shown to achieve 95% clinical sensitivity and 100% specificity for reading out via a standard benchtop fluorescence scanner [11]. However, there could be several problems with these Au NPs-based LFAs: i) gold is an expensive material and its production is plateauing [12]; ii) the demand of metallic NPs market is expected to double within the next decade, from ~USD 2.4 billion in 2021 up to ~USD 4.2 billion in 2030, with an annual growth rate of ~12% [13]; and iii) the final price for the chemical synthesis of Au NPs depends not only on the value of the bulk material but also on their production cost. As an example, colloidal Au NPs is estimated to have their manufacturing cost to be ~10^5 higher than the price of the bulk material [14]. So, in a field and market dominated with noble metal NPs [8], alternatives materials are needed, better yet if they are inexpensive for having more affordable technologies. Then, custom-made plasmonic NPs can provide a suitable alternative for current over-the-counter testing.

Alternatives -more abundant and less expensive- plasmonic NPs, such as copper and transition metal nitrides, and others, arise as promising optically active alternatives [15], especially in the field of nanomedicine. Here we focus on the biofunctionalization and subsequent LFA implementation with spherical copper nanoparticles covered with a gold shell (Cu@Au) and spherical titanium nitride (TiN) NPs, as they have been proved to be stable, bio-friendly and capable of being manufactured at large scale [16-19]. These two particular materials bring benefits such as low cost and abundance. On the one hand, TiN has proved to be a good plasmonic material in the vis/NIR region, and additionally is a good refractory material, with a high melting point and high chemical stability in harsh environments [20]. On the other hand, bare Cu-structures show an interband transition energy level of 2.15 eV, hence having the capability of interband excitation within the visible range, although oxidation of their surfaces is still an issue [21].

TiN NPs show a plasmonic peak in the range of 650-800 nm and high photothermal conversion efficiency [15, 22]. Nevertheless, their biomedical application has been limited due to the difficulty of fabricating large-scale spherical-shaped in water, until now. We recently demostrated femtosecond laser ablative synthesis of large amounts of such high quality TiN NPs [17, 19, 23], with already proven bioefficiency in low toxicity *in vitro* and *in vivo* [17, 18], photothermal therapy on U87–MG cancer cell cultures under near-infrared laser excitation [17], and photoacoustic biological imaging [23]. In general, laser-synthesized TiN NPs present a safe choice for future biomedical applications, especially since they show superior photothermal and photoacoustic features compared to typical plasmonic counterparts [24, 25]. Moreover, ultrastable Cu@Au NPs on the other hand, have been recently synthetized via a seed-mediated galvanic replacement approach, which unlike CuAu alloys, the thin Au shell here provides enhanced stability. Furthermore, they show a superior photothermal efficiency in solar-induced water

evaporation as compared to Au NPs [16]. In general, TiN and Cu-Au NPs are promising to be useful in several fields such as catalysis, light harvesting, optoelectronics, and biotechnologies [26-29].

Here we show that inexpensive plasmonic TiN- and Cu@Au-based LFAs perform comparable to Au NPs-based LFAs, in some cases even better. Firstly, we transfer both kinds of NPs from their original synthetization solvents (acetone and hexane) to biofriendly solvents, such as water and Tris-EDTA (TE) buffer, to be usable in LFA technology. Then, the performance of antibody-functionalized TiN and Cu@Au NPs for detecting two kinds of biomolecules, Fluorescein isothiocyanate (FITC) and cardiac troponin (cTnT), was characterized on LFA strips. Our results show that the binding of the functionalized Cu@Au and TiN NPs allows an easy visualization of the target protein by naked eye and providing a signal efficiency and specificity similar to the observed when using the Au NPs. We further confirm these signals with machine learning techniques. Our approach could be just a starting point for the massive usage of these inexpensive NPs in bio-applications, in where the NPs plasmonic features in combination with their successful functionalization capabilities, may be useful in photothermal therapies, delivery, imaging and sensing technologies.

Results

COMSOL Multiphysics® simulations.

Numerical simulations were carried out in order to assess and quantify the optical performance of our three kinds of NPs, performed with COMSOL Multiphysics® software. Briefly, these are classical electromagnetic simulations for optically-excited NPs, performed via

the Finite Elements Method with COMSOL. We simulate illumination of the NPs with linearly polarized light (Eqs. 1-3) and calculate the optical extinction response of the system, which is the computational counterpart of the experimental absorbance measurements. The optical extinction was fitted to the experimental absorbance, finding excellent agreement, which was later used to calculate the day-vision visible parameter. See full details in the Materials and Methods section and Section I of Supplementary information and Figure S1. The anticipated optical performance between these NPs can be estimated if there is a similarity in the magnitude of the day-vision parameter given by Eq. 4, defined as the ability for the NP with a given spectra to be "seeable" by the human eye during the day. The day-vision parameter is calculated by the convolution between the eye's day vision sensitivity (shaded-bell color in Fig. 1B) and each NPs' individual absorbance (plasmons in 1B), yielding the efficiencies shown in Fig. 1C. The calculation started with fitting the numerical absorbances with our experimental absorbances, from where then the first were used in Eq. 4. The calculated parameters indeed show a similar order of magnitude quantities, anticipating that both TiN and Cu@Au NPs should be as good color signal within the visible range as Au NPs.

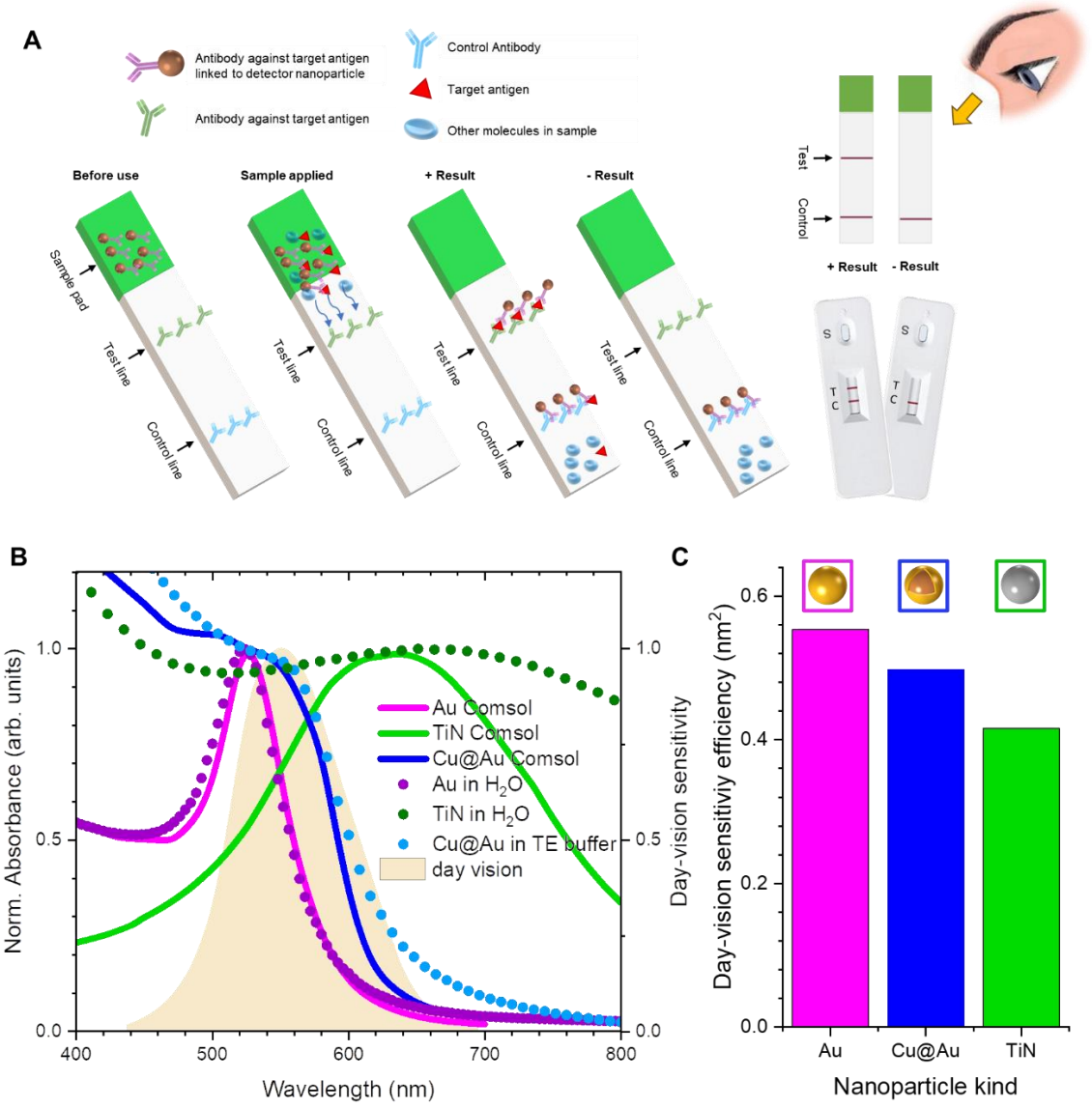

Figure 1. (a) Schematic representation of a lateral flow assay (LFA) showing the sample pad containing the marked antibody against the target antigen and the test and control lines. After the sample is applied to the sample pad, the sample plus the antibodies diffuse through the strip. Only if the target antigen is present, the marked antibody will bind to both the test and control lines (+ result). If the target antigen is not present, the target antibody will only bind to the control line (- result). The binding of the target antibody to the control line is necessary to validate a LFA test. (B) Extinction cross sections from computational simulations for Au, TiN, and Cu@Au, all in a water environment (ε_{NP} =1.8) and each NP for diverse experimentally characterized sizes of 40 nm, 30 nm (28 nm TiN and 2 nm of TiO2 shell), and 12 nm (11.5 nm of Cu and 0.5 nm of Au shell), respectively. The shaded area shows the day-vision sensitivity of the human eye (photopic vision), $V_{day-vision}(\lambda)$. (C) Day-vision sensitivity efficiency parameter for each NP as shown, anticipating similar performance in visual-assessment devices.

Cu@Au and TiN NPs preserved their characteristics after being transferred to aqueous solvent.

The ultra-stable copper NPs with a thin shell of gold (Cu@Au) were synthesized via galvanic replacement. The Cu@Au NPs were dispersed in hexane and contained a coating layer of oleylamine. During their characterization, Wang et al described that these ~12 nm particles showed high stability even in harsh environment since the gold shell was completely protecting the copper core [16]. The TiN NPs were synthesized via laser ablation, a method that allowed the production of large amount of spherical size specific NPs, which do not tend to aggregate due to electrostatic stabilization [17]. These stable NPs of ~30-40 nm were grown in acetone, showing great stability and they already showed capability of being covered by polyethylene glycol [17, 19, 23]. However, to be used in biological devices, it is more convenient to preserve these NPs in aqueous solvent but maintaining their original characteristics. As depicted in Figure 2, we were able to successfully transfer the Cu@Au and TiN NPs to aqueous media by ligand exchange and evaporation of acetone, respectively. The characterization of the Cu@Au NPs indicates that these particles have an average size of 12 nm (Weibull fit, max. 11.3nm) when suspended in the aqueous medium (Fig. 2A). After measuring absorbance, the observed plasmon was around 555 nm, which corresponds to the plasmon observed for these NPs when synthesized and suspended in hexane (Fig. 2B). We also analyzed the stability of the NPs in the aqueous medium and compared it to the stability of these particles in hexane. The plasmon measured at day zero and >40 days, indicate that the stability of the Cu@Au NPs suspended in aqueous medium is preserved since no notable changes in the absorbance were observed (Fig. 2C). The characterization of the TiN NPs indicates these particles have an average size of 35 nm (Weibull fit, max. 34.5nm) when suspended in water (Fig. 2D). After measuring the absorbance, the observed plasmon was around 650 nm, in good agreement with the observed plasmon before transferring the NPs to water (Fig. 2E). As with the

Cu@Au NPs, the TiN NPs were also stable through time since their plasmon was preserved after >40 days (Fig. 2F). Together, these results show that after transferring the Cu@Au and the TiN NPs to an aqueous medium, the size and optical properties of the Cu@Au and TiN NPs were preserved, being eventually useful in time-sensitive distribution.

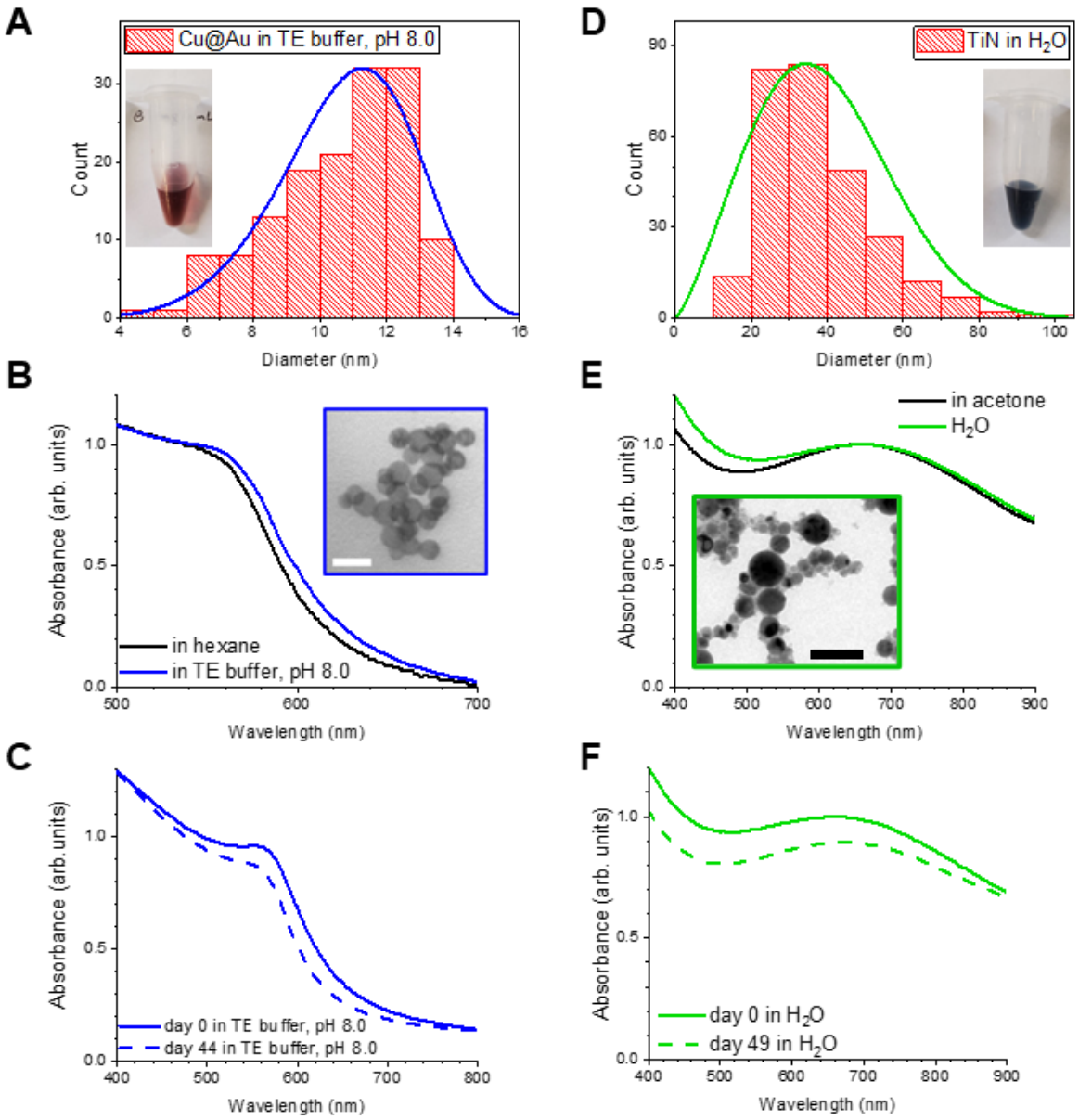

Figure 2. Characteristics of Cu@Au and TiN NPs after their transfer to bio-compatible aqueous media. (A) Plot showing the TEM size distribution of the Cu@Au NPs after their transfer to an aqueous medium. The inset shows a visual of the post-transfer solution. (B) Plasmon of Cu@Au NPs in hexane and aqueous medium. The inset shows a representative TEM image displaying that the NPs show minimal aggregation after being transferred to TE buffer (Bar 20 nm). (C) Conservation of the plasmon through time of the Cu@Au NPs dispersed in TE buffer. (D) Plot showing the TEM size distribution of the TiN NPs after their transfer to water. The inset shows a visual of the post-transfer solution. (E) Comparison of TiN's plasmon in acetone versus water. The electron microscopy inset confirms that the NPs do not aggregate after acetone evaporation (Bar 100 nm). (F) Conservation of plasmon through time of the TiN NPs.

Functionalized Cu@Au and TiN NPs showed similar efficiency to Au NPs in LFA.

To determine if these NPs could have bio-applications such as being used as biosensors, we tested if they can be functionalized with antibodies and used to detect an antigen of interest. For the analysis, we functionalized the Cu@Au and the TiN NPs with an antibody anti-FITC. As a control, the commercial 40 nm Au NPs (NanoComposix®) were used and tested at the same time. We first selected the appropriate buffers for each NPs ensuring that the buffer does not induce the aggregation and precipitation of the NPs during the functionalization process. As shown in Figure 3A, after functionalization, the control Au NPs and the Cu@Au and TiN NPs were maintained in homogeneous suspension. To corroborate their functionalization, we measure their absorbance before and after functionalization. As shown in Figure 3B, all the NPs showed a plasmon shift after functionalization, suggesting a few nm new shell of new dielectric media (in our case, biomolecules), evidence of a successful modification step. Moreover, the efficiency of the functionalization was similar for the three NPs, as demonstrated by their absorbances (Fig. 3B). For testing the ability of these NPs to detect the antigen of interest, we run LFA using each of the functionalized NPs. As shown in Figure 3C, the functionalized TiN and Cu@Au NPs were able to identify the target protein (FITC-T10-Biotin) present at a concentration between 100 and 1 nM. We also quantified the intensity of each LFA band for the Au/Cu@Au and TiN NPs, determining that the intensity of the signal given for the TiN NPs was similar to the intensity registered when using the Au NPs (Fig. 3D). The intensity of the LFA bands observed when using the Cu@Au NPs (~12 nm) was ~37% lower compared to the Au NPs (Fig. 3D). However, considering the size of the tested particles, our results indicate that both NPs, Cu@Au, and TiN, can be successfully functionalized and effectively detect a specific target protein with similar or even better efficiency to the very well-standardized Au NPs. The plasmonic characteristic of the NPs was preserved even

when attached to the test and control line of the LFA strip, as demonstrated by their ability to absorb at specific wavelength [see Figure S2].

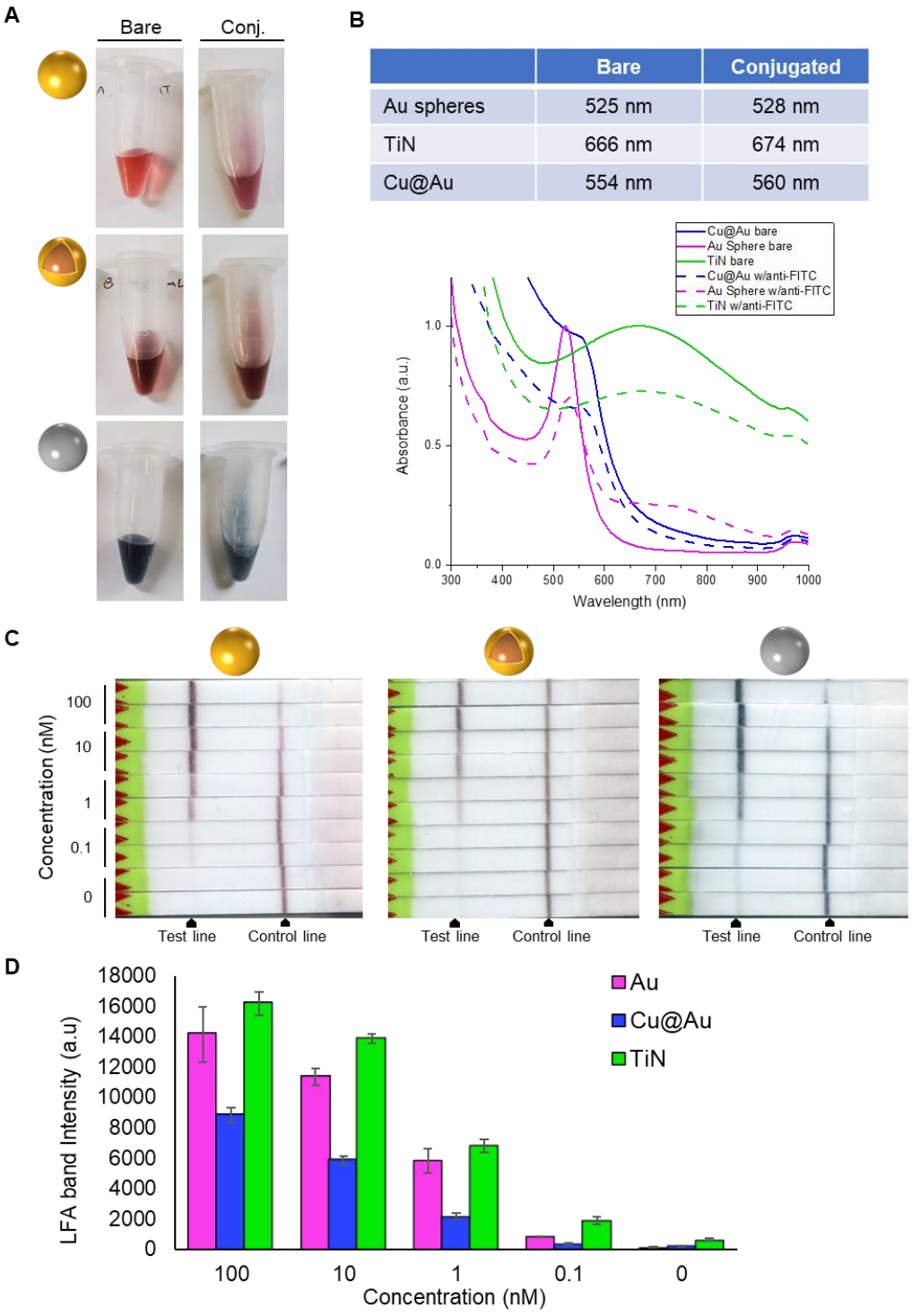

	Bare	Conjugated
Au spheres	525 nm	528 nm
TiN	666 nm	674 nm
Cu@Au	554 nm	560 nm

Figure 3. Functionalization of NPs with anti-FITC antibody. (A) Visual characterization of each type of NPs before and after antibody conjugation to demonstrate they do not aggregate nor precipitate. (B) Table and plot comparing the plasmons for each type of NPs before (solid lines) and after (dashed lines) conjugation. (C) LFA in duplicate showing the identification of FITC at different concentrations (100, 10, 1, 0.1, and 0 nM) using the conjugated NPs. (D) Plot showing the intensity measured via ImageJ of each test band of the LFA.

Functionalized Cu@Au and TiN NPs can detect proteins with biological significance.

Since our first functionalization analysis involved the conjugation of the antibody anti-FITC and the recognition of the system FITC-T10-Biotin, we tested if the particles can be functionalized and detect proteins with biological significance. Here, we functionalized the NPs for detecting cardiac troponin (cTnT), that is a protein that increases in the blood of patients that are suffering a heart attack. Both the Cu@Au and the TiN NPs were modified with an antibody anti-cTnT together with the Au NPs which was our positive control. As observed in Figure 4A, a change in the migration pattern in a 0.25% agarose gel confirms the functionalization of the Cu@Au and TiN NPs. Additionally, the visual analysis of the NPs solution confirms that the NPs do not aggregate during the process of conjugation (Fig. 4A). We also did TEM imaging for the Cu@Au NPs after functionalization, where we can see they do not aggregate and remain mono-dispersed [see Figure S3A]. In addition, and as shown in Figure S4, a shift in the Cu@Au and TiN NPs absorbance pattern further confirms their successful functionalization. Next, to corroborate the ability of the modified NPs to recognize the protein of interest, different concentrations of recombinant human cTnT were blotted in a nitrocellulose membrane as displayed in the scheme from Figure 4B. After blotting, the presence of the proteins in the nitrocellulose membrane was confirmed by Ponceau S staining (Fig. 4C, left picture). The membrane was then divided into three equal pieces and each of them was incubated with one of the NPs. As shown in Figure 4C (right), after the incubation of the nitrocellulose membranes with each of the functionalized NPs, we confirmed that the three conjugated NPs (Cu@Au, TiN and the control Au) were able to bind to the target protein (cTnT), displaying a signal that correlates with the amount of protein blotted in the membranes. The signal was observed quickly, after 10 minutes of incubation with each NP (picture was taken after 30 minutes of incubation). These results confirm that the TiN and the

Cu@Au NPs can be functionalized with different antibodies for being able to identify target proteins with biological significance. Finally, to test the specific recognition of the target protein, LFA was developed as displayed in the scheme from Figure 4B, using bovine calf serum with (+) or without (-) cTnT (0.03 ug - 0.04 ug). Each LFA confirms the specificity of the test since the test bands were only observed in the presence of cTnT (Fig. 4D). The binding of the functionalized Cu@Au and TiN NPs allow the easy visualization of the target protein by the naked eye, with a signal efficiency and specificity similar to the observed when using the Au NPs (Fig. 4C and D).

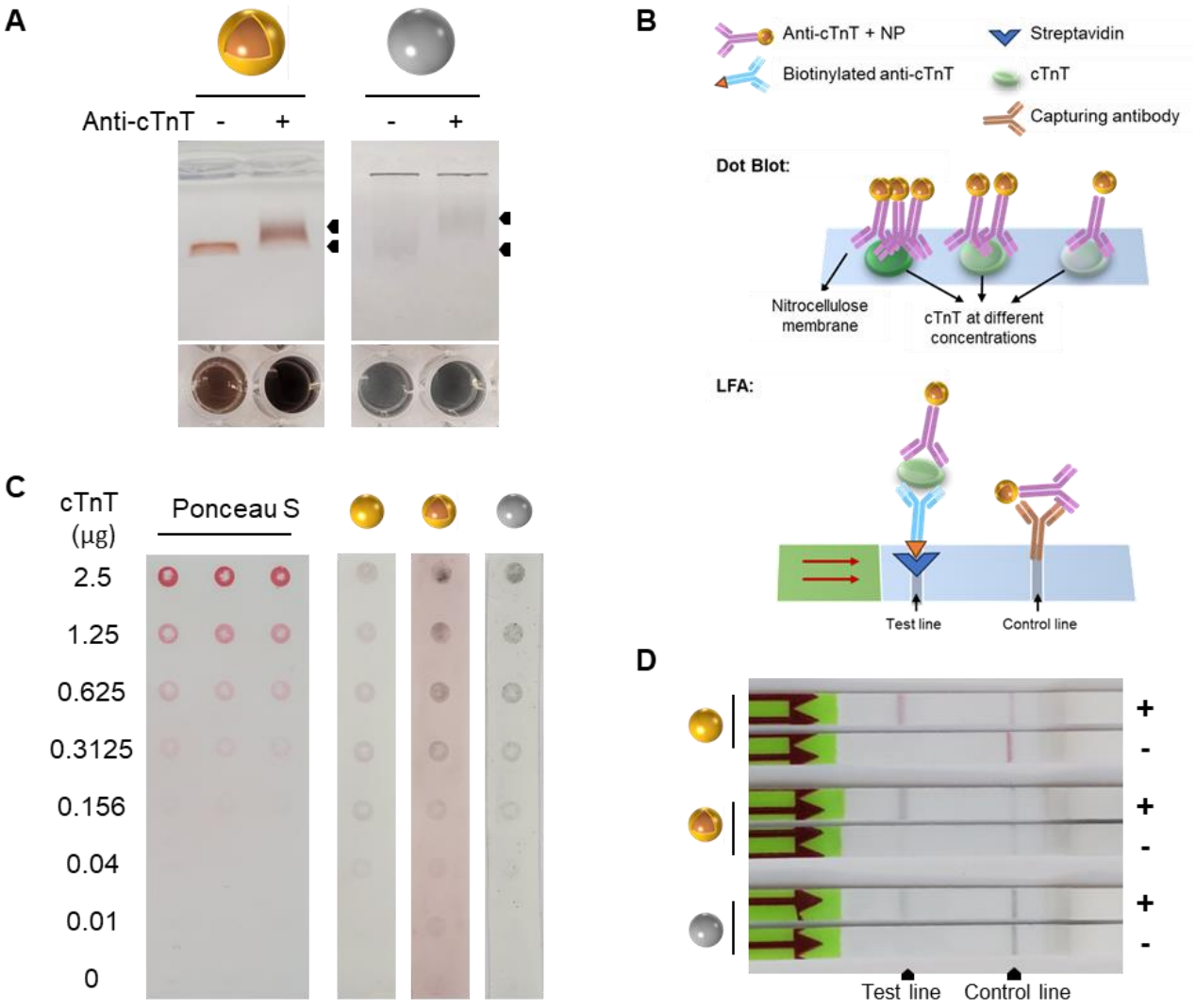

Figure 4. Using Cu@Au and TiN functionalized NPs for naked-eye detection of cardiac troponin. (A) 0.25 % agarose gel for testing the functionalization of the Cu@Au and TiN NPs. At the bottom of the gel, each solution pre- and post-functionalization is shown. (B) Representative schemes of the dot blot (top) and LFA (bottom) used for testing, respectively, the ability of the Cu@Au and TiN NPs to detect the target protein and their specificity. (C) Dot blot analysis showing the detection of cardiac troponin (cTnT) at different concentrations (µg). The Ponceau S staining corroborates the presence of cTnT at different concentrations in the nitrocellulose membrane. The membrane was cut into 3 sections, which are shown after being incubated for 30 minutes with the conjugated Au, Cu@Au, and TiN NPs. (D) LFA against cTnT diluted in bovine calf serum, showing the specific detection of cTnT when using each conjugated NP.

Common machine learning platform and experiments to evaluate Cu@Au and TiN-based LFAs in the detection of FITC.

The aim of this section is to establish a common and fair machine learning platform for comparing the discriminative capabilities of the proposed TiN and Cu@Au-based LFAs against Au-based LFAs. Toward this objective, we developed two methods. The first method involves feature extraction based on the Red-Green-Blue (RGB) color channels of the test and control lines on the strips. The second method employs contrastive learning, an advanced machine learning model, to enhance feature extraction. The K-Nearest Neighbor (K-NN) classifier is utilized in both methods to perform strip classification into three categories: TiN, Cu@Au, and Au.

The dataset for our machine learning experiments consists of three types of NPs: TiN, Cu@Au, and Au. Within each NP category, pairs of strips were tested with six different concentrations of FITC. We manually segmented the test and control lines on each strip, focusing on their central areas as depicted in Fig. 5A. The Red/Green/Blue (R/G/B) channels of all lines were fitted with Gaussian distributions, from which we extracted the mean, along with the lower and upper bounds of the first standard deviation. Each line is represented as a nine-element vector, and each strip's representation is an 18-element vector, formed by concatenating the vectors of the test and control lines.

A group-wise k-nearest neighbor (k-NN) model is employed to assess the discriminative capability of the NPs. Within each NP group (TiN, Cu@Au, Au), a pair of strips with the same concentration is randomly assigned for either training or testing, resulting in six strips for each set in each NP group. We use k = 1 in the k-NN algorithm, as each class consists of only one sample (strip). Figure 5C shows the accuracy results for the different NPs, indicating that TiN and Cu@Au

achieve higher accuracy compared to Au. This can be considered evidence that TiN and Cu@Au LFAs are more robust and responsive in detecting FITC concentrations.

In this work, we developed an advanced feature extraction approach known as contrastive learning to further explore the discriminative capability of the NPs. Contrastive learning uses negative sampling and contrastive loss functions to effectively distinguish between different classes or categories of data. In our experiment, we grouped the strips based on their FITC concentrations. Our contrastive learning model employs a Siamese network [30] consisting of two identical subnetworks, each with a simple architecture that includes a single fully connected layer. This Siamese network processes a pair of strips from the training set, generating two corresponding vectors, as shown in Fig. 5B. We then apply the k-NN classification method, using the same experimental setup as in our previous experiment. The results of this approach are shown in Fig. 5C. Through the application of contrastive learning, both Cu@Au and Au demonstrated improved performance, while TiN's performance remained unchanged. However, the accuracy for TiN and Cu@Au still surpassed that of Au, indicating that the features of TiN and Cu@Au-based LFAs are more distinguishable.

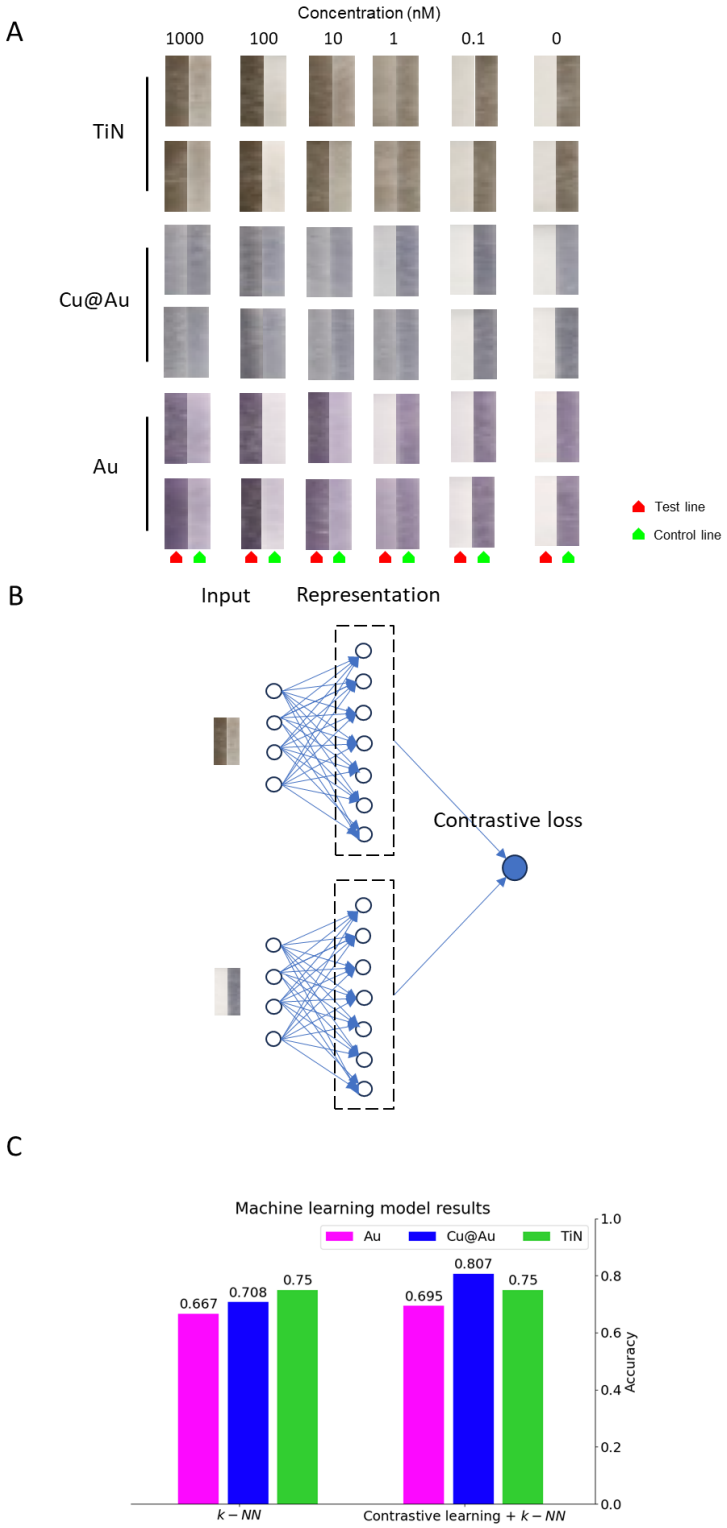

Figure 5. Data, models, and results of our machine learning experiments. (A) Cropped test lines and control lines of all strips that tested with different FITC concentrations. (B) Siamese network-based contrastive learning method. (C) Results of the machine learning experiments. It is evident that the accuracy of TiN and Cu@Au-based LFAs surpasses that of Au-based LFAs.

Discussion

The COVID-19 pandemic showed the utility of the easy to develop and affordable LFA tests. These tests are made mostly of gold, a noble metal with great chemical stability and strong plasmonic absorption. However, price and global availability are some issues that can affect its massive use in close future. Indeed, gold is an expensive material with a weak natural abundance, while the use of chemical methods for the fabrication of Au NPs leads to a further drastic increase of the cost of biomolecular labels. In this study, we proved that TiN and Cu@Au NPs-based LFAs perform comparable to Au NPs-based LFAs. Our data shows that these particles can be dispersed in an aqueous medium (Fig. 2), facilitating their use not only as a biosensor but for other technologies that require the use of biocompatible mediums and plasmonic characteristics. In this work, we firstly show that these novel inexpensive NPs can be successfully transferred to bio-friendly medium for later biological uses (Fig. 2C-D), where it was shown that these NPs are stable as a function of time (Fig. 2E-F), so they could be eventually used in long-times delivery operations. We then show that both NPs, TiN and Cu@Au can be successfully functionalized with diverse antibodies, clearly demonstrated by the change in the plasmon peaks and agarose gel analysis (Figs. 3 and 4). Furthermore, the antibodies conjugated to the TiN and Cu@Au NPs preserve their function, confirmed by the identification of different concentrations of FITC (Fig. 3) and cTnT (Fig. 4).

Antibody orientation onto NPs is an important factor that has been broadly studied and discussed [31-34] since the proper orientation of an antibody on the NPs surface preserves the antibody ability for detecting specifically the target molecule. Au NPs have demonstrated this ability, which is also shown in this study for the TiN and Cu@Au NPs. The conjugation of TiN NPs, as well as for Au control NPs, involved the non-covalent immobilization of the target

antibody onto their surfaces. However, this mechanism does not work with the Cu@Au NPs due to the presence of the carboxyl groups from the 3-MPA. Then, to ensure the proper conjugation of the Cu@Au NPs, in this study we included EDC, which reacts with the carboxyl group of the 3-MPA, followed by the incorporation of a hetero-bifunctional crosslinker containing an amine-reactive N-hydroxysuccinimide (NHS) ester and a photoactivatable nitrophenyl azide, mediating the covalent interaction between the NP and the target antibody. In addition, conjugation of the TiN NPs with DNA via instant dehydration in butanol [35] was tested as shown in Figure S3B, demonstrating the versatility and stability of the conjugation process given by these NPs. By the successful conjugation and identification of two different markers, our results also prove that the TiN and Cu@Au NPs allow working flexibility, like the one provided by the Au NPs. This working flexibility is an important characteristic since indicates that these less expensive NPs can be broadly used in biotesting technologies as the Au NPs are currently being used. Additionally, as shown in figure 4, when the conjugated NPs were exposed to a sample containing not only the target protein, but a mix of proteins contained in the bovine calf serum, the specific detection of the target protein confirms that the TiN and Cu@Au NPs have similar properties compared to the Au NPs.

Our result also demonstrates that the signal provided by these novel NPs at naked eye examination is comparable to the signal provided by the Au NPs, as it was qualitatively predicted by our simulation via COMSOL Multiphysics® (Fig. 1). In this simulation, the NPs' signal similarity of the day-vision parameter given by Eq. 4, which anticipated how "seeable" the NPs-loaded LFA lines will be, correlates with our experiments. However, when compared to the measured experimental intensities, we can see slight differences between the anticipated values in Fig. 1C and the optical intensities measured in Figs. 3 and 4. The experimental measured lower

signal of the Cu@Au NPs-loaded LFAs could be explained by the smaller size of these NPs, since we used the same NP concentration in the tests and the surface area of a single Cu@Au NP was about 90% less than that of single Au and TiN NPs. We expect that if we use same mass of NPs for the tests, the Cu@Au NPs can outperform the Au NPs. On the other hand, the experimental higher signal of the TiN NPs-loaded LFAs could be explained by the polydispersity of larger size of these NPs shown in Fig. 2D. Furthermore, the results from the dot blot and LFA of Figs. 3 and 4, demonstrate that the observed signal correlates with the amount of target protein, which suggests that after a suitable numerical preparation and subsequent experimental standardization, this technique can be apply not only for determining the presence or absence of a biomolecule, but also for a more quantitative analysis.

We should also comment on other inexpensive alternatives available on the current market. Cheaper materials already exist in the context of LFAs, such as latex, polystyrene and carbon, among others. However, several of these devices require sophisticated equipment for reading out the results, hence delaying a possible diagnosis. For example, even though remarkable advances for low concentrations sensitivity and quantitative detection have been achieved in polystyrene microspheres-based LFAs for troponin detection, these still need to be quantified with a fluorescence benchtop reader [36-38]. More recently, latex beads-based LFAs were proposed for achieving sensitivities in the order of ~ng mL^{-1}, but the readout was done via a commercially available optical LFA reader [39]. Additionally, these materials do not show the benefits of plasmonic systems our NPs present, such as e.g., propagating/localized surface plasmon resonance (SPR), surface-enhanced Raman scattering (SERS), surface-enhanced fluorescence and surface enhanced infrared absorption spectroscopy, among others [40]; which broadens the possible applications in where our NPs could be used.

As for our machine learning approach, and by considering our notably limited dataset, which includes only a pair of strips for each NPs type at the same FITC concentration, the simple k-NN algorithm obtains an accuracy higher than 70% for TiN and Au@Cu-based LFAs. Through contrastive learning, the accuracy surpasses 75%. The visual features exhibited by TiN and Cu@Au-based LFAs prove to be robust, responsive, and consistent in detecting various FITC concentrations, indicating their potential as viable alternatives to Au-based LFAs with broader applicability in bio-related domains. Moreover, the accuracy obtained in our machine learning experiments, despite the constraints of very limited data, suggests the potential for automated quantitative analysis of biomolecules using TiN and Cu@Au-based LFAs.

In conclusion, we demonstrate here that the performance of these less expensive (TiN and Cu@Au) NPs for detecting FITC and cTnT, was similar to the performance of the current gold standard Au NPs. For the machine learning approach, the TiN NPs show an advantage in recognition accuracy that speaks to the potential of new materials in biosensing.

Acknowledgements

V.A.B.L. and S.W. acknowledge the partial support by NIH ES030425 (to S. W.) and the Edison Biotechnology Institute, Ohio University (V.A.B.L. and S.W.). O.A.O. and A.O.G. acknowledge the generous financial support from the Baker Fund, QBI, and NQPI at Ohio University. E.S. and K.L.A.C. acknowledge the Department of Chemistry and Biochemistry and the College of Arts and Sciences. D.M. is grateful to the support of Canada Research Chairs Program (CRC 950-232964), Natural Sciences and Engineering Research Council of Canada (RGPIN-2020-05921) and the Fonds de recherche du Quebec-Nature et technologies.

Materials and Methods

Computational simulations. Our classical electromagnetic simulations on plasmonic nanoparticles are performed via the Finite Elements Method with the COMSOL Multiphysics simulations software. We illuminate the nanoparticle with linearly polarized light and calculate the optical response of the system. The incident electromagnetic field is defined as: $\vec{E}_{\text{ext}} = \text{Re}\left[\vec{E}_0 e^{i\omega t}\right]$. By solving the Maxwell's equations within a classical framework, the calculations provide far-field quantities such the absorption (σ_{abs}), scattering (σ_{scat}), and extinction (σ_{ext}) optical cross-sections (related by $\sigma_{\text{ext}} = \sigma_{\text{abs}} + \sigma_{\text{scat}}$). The scattering cross-section is calculated by integrating the scattered intensity over a fictitious sphere around the NP, whereas the formalism for the absorption cross-section is based on the following equations:

$$Q_{\text{abs}} = -\text{Im}(\varepsilon_{\text{NP}})\frac{\varepsilon_0 \omega}{2}\int \text{d}V \ \vec{\text{E}}_\omega \cdot \vec{\text{E}}_\omega^{*}, \qquad (1)$$

$$\sigma_{\text{abs}} = \frac{Q_{\text{abs}}}{I_0}, \qquad (2)$$

where Q_{abs} is the absorbed power by the system, ε_{NP} is the dielectric constant of the metal nanoparticle, ω is the angular frequency of the incident light, $\vec{\text{E}}_\omega$ is the complex electric field inside the metal, and I_0 is the photon flux magnitude (intensity for simplicity), given by

$$I_0 = \frac{c_0 \varepsilon_0 \varepsilon_{\text{med}}^{1/2}}{2}\left|\vec{E}_0\right|^2, \qquad (3)$$

where ε_{med} is the dielectric constant of the medium, c_0 is the speed of light in vacuum, ε_0 is the vacuum permittivity, and $\left|\vec{E}_0\right|$ is the electric field magnitude of the incident electromagnetic wave. All NPs are simulated with sizes estimated from experimental characterization, as described in

Fig. 1. In particular, for TiN NPs we find that a thin shell of TiO_2 is needed in the accurate simulation of the extinction, as previously described elsewhere [41]. For gold and copper we use the permittivity $\varepsilon_{\mathrm{NP}}$ from Johnson and Christy [42], for TiN from Guler [43], and for TiO_2 from Siefke [44]. The sum of σ_{scat} and σ_{abs} allows to obtain σ_{ext}, related to the experimental measurement of absorbance.

We also calculate the day-vision optical sensitivity for each NP, given by

$$\mathrm{Efficiency}_{day-vision} = \frac{\int \sigma_{\mathrm{ext}}(\lambda) V_{day-vision}(\lambda)\,\mathrm{d}\lambda}{\int \sigma_{\mathrm{ext}}(\lambda)\,\mathrm{d}\lambda}, \qquad (4)$$

which allows us to estimate how good each NP will perform on a test based on visual assessment under normal day light conditions.

Synthesis of Cu@Au NPs. Typically, 33.2 mg of copper(II) acetylacetonate ($Cu(acac)_2$, ⩾99.9%, Sigma-Aldrich) was dissolved in 10 mL of Oleylamine (OLA, 70%, Sigma-Aldrich) under nitrogen atmosphere. Then, the solution was kept at 230 °C for 3 h to produce Cu NPs. Subsequently, the solution was cooled down to 140 °C and then 1 mL of Trioctylphosphine (TOP, 90%, Fisher Scientific) solution of gold(III) chloride trihydrate ($HAuCl_4 \cdot 3H_2O$, ⩾49.0%, Sigma-Aldrich) (20 mg) was injected. After 1 h reaction, the solution was quickly cooled down to room temperature. Finally, the Cu@Au NPs were purified and dispersed in hexane for further use.

Cu@Au NPs ligand exchange. 1 mL of Cu@Au dispersion in hexane was added to 2.5 mL of methanol. The solution was alkalinized by adding 140 µL of NH_4OH (Sigma). Then, dropwise, 90 µL of 3-Mercaptopropionic acid (3-MPA, Sigma) was added. The solution was heated in a hot plate at 75°C for 1h with manual sporadic agitation to yield the 3-MPA capped Cu@Au NPs. The NPs were then precipitated by adding 10 mL of distilled water, 2.5 mL of isopropanol, and 1%

Triton x100. The Cu@Au NPs were collected by centrifugation at 7000 rpm for 10 min, rinsed with water, and resuspended in 1X Tris-EDTA (TE), pH 8.0 buffer.

TiN NPs synthesis. TiN NPs were synthesized by the technique of femtosecond laser ablation in liquid ambient. A TiN target (MaTeck, Germany, 99+%) was fixed in a vertical position inside a glass cuvette (Hellma, Germany, optical glass, 88 mL, 2.5 mm wall thickness) filled with 80 mL of acetone (Acros Organics, 99.5+%). The thickness of the liquid layer between the target and a cuvette wall was 3 mm. To initiate material ablation, a femtosecond laser beam (s-Pulse HP, Amplitude Systems, France, Yb:KGW, 490 fs, 10 kHz) was focused through the cuvette wall on the surface of the target using a 75 mm convex lens. The energy was attenuated down to 150 μJ per pulse using a half-wave plate and Brewster polarizer. To prevent ablation from the same area, the target was constantly moved at a speed of 2.5 mm s^{-1} by a translation stage (scanned area was 5 x 5 mm^2).

TiN NPs water dispersion. Distilled water was added to a TiN dispersion in acetone in a ratio of 1:1. The mixture was heated on a hot plate at ~150°C under constant agitation until all the acetone was evaporated from the sample.

Electron microscopy. NPs drop-cast from solution onto Lacey Carbon TEM grids to facilitate various types of NP characterization. A JEOL 1010 Transmission Electron Microscope (TEM) operated at 80 kV and connected to a MSC TK1024M camera (Gatan, Munich, Germany), was used to obtain the NPs morphological details.

Functionalization of NPs with FITC. NPs were centrifuged and dispersed in their corresponding buffer (Au: TE pH 8.0, Cu@Au: Borate pH 7.0, and TiN: 1X TE pH 8.48). 2 μg of anti-FITC (200-032-037, Jackson ImmunoResearch Laboratories, Inc.) per 40 μL of NPs solution was added and

incubated in a rotor at 4°C for 30 min. 10% BSA was added to the NPs to have a BSA final concentration equal to 1 %. The samples were incubated for an extra hour at 4°C with constant rotation. The NPs were then rinsed twice and centrifuged at 13,000 rpm for 10 min each. Finally, the NPs were resuspended in their corresponding buffers.

Functionalization of NPs with anti-cTnT. Au and TiN NPs were centrifuged and then dispersed via sonication in their corresponding buffer (Au: 1X TE pH 8.0 and TiN: 1X TE pH 8.48). 10 µL/mL of Anti-Cardiac Troponin T antibody [1F11] (cTnT, ab10214, Abcam) was added to each sample and incubated in a rotor at room temperature for 30 min. 10% BSA was added to the NPs to obtain a BSA final concentration equal to 1 %. The samples were incubated for an extra hour at room temperature with constant rotation. The NPs were then rinsed twice and centrifuged at 4 °C and 12,000 rpm for 10 min each. Finally, the NPs were resuspended in their corresponding buffers. For the Cu@Au NPs, after centrifugation, NPs were resuspended in 100 mM MES buffer pH 6.0 containing excess of freshly prepared 1-Ethyl-3-[3-dimethylaminopropyl]carbodiimide hydrochloride (EDC, 1 mg/mL, # 22980, Thermo Scientific™). Excess of sulpho-sulfosuccinimidyl 6-(4'-azido-2'-nitrophenylamino)hexanoate (sulpho-SANPAH, 1 mg/mL, # 22589, Thermo Scientific™) was added immediately to the NPs solution and samples were incubated in dark, at room temperature and under constant rotation for 20 min. 2-Mercaptoethanol (10 µL/mL) was added to the NPs to quench EDC, samples were incubated under the same condition for an additional 20 min. Same volume of 100 mM phosphate buffer pH 7.5 was added to increase the pH of the Cu@Au NPs, following for 10 µL/mL of anti-cTnT antibody (ab10214, Abcam). Samples were transferred to a flat container and irradiated with UV from a 340-UVA lamp (Q-lab, Co.) for 45 minutes at 1.15 mW/cm^2. NPs were centrifuged at 12,000 rpm and 4 °C for 10 minutes and rinsed in 1X TE buffer pH 8.0.

Agarose gel separation. 0.25 % agarose gel was prepared in 0.5 X Tris-borate-EDTA (TBE) buffer (40 mM Tris-base, 40 mM Boric acid, and 1 mM EDTA). The samples were loaded with sucrose 50 % and run at 100 Volts for 5 to 10 min.

Lateral flow assay (LFA). For FITC-LFA, 20 µL of anti-FITC functionalized NPs were mixed with 0.2 µL of the oligo FITC-T10-Biotin (Metabion International AG, Germany) diluted at the specified concentrations. Commercial LFA strips (MGHD1, Milenia GenLineHybridetect, Germany) were used, which were produced at request without the gold NPs pad. The samples were run following the manufacturer's indications. The strips were scanned and the intensity of each band in the test strips was quantified using Image J. For cTnT LFA, commercial LFA strips (MGHD1, Milenia GenLineHybridetect, Germany) were loaded with 4 µL (Au/TiN) or 8 µL (Cu@Au) of conjugated NPs (OD ~1.0). 10 µL (for Au/TiN LFA) or 13 µL (for Cu@Au LFA) of sample mix (50 µL of running buffer, 25 µL 1:1 bovine calf serum/PBS containing 0.156 µg of recombinant human cTnT (ab86685, abcam), and 1 µL of biotinylated anti-cTnT antibody [bs-10648R-Biotin, Bioss]) was loaded in the LFA strips. The sample mix for the negative controls only contains running buffer, biotinylated anti-cTnT antibody and bovine calf serum in PBS (1:1).

Dot blot. Recombinant human cTnT (ab86685, abcam) was diluted in 1X PBS buffer. 50 µL of the protein at different concentration were blotted onto a nitrocellulose membrane (0.2 µm, #88024, Thermo Scientific™). After aspiration was completed, the membranes were stained with Ponceau S to check the presence of the blotted protein on them. The membranes were rinsed with TBS-T buffer until completely removed the stain and then blocked in 5 % milk for 30 minutes. The membranes were rinsed once with each of the corresponding NPs-buffers followed by the incubation for a maximum of 30 min at 4°C with the conjugated NPs.

Author contribution

Veronica A. Bahamondes Lorca: Bioconjugation of NPs, LFA testing, NP's ligand transfer, conceptualization, and manuscript writing, **Oscar Ávalos-Ovando**: Bioconjugation of NPs, LFA testing, simulations, conceptualization, and manuscript writing, **Christoph Sikeler**: Bioconjugation of NPs, LFA testing, conceptualization, imaging, manuscript writing, **Eva Yazmin Santiago**: simulations, **Eli Skelton**: UVvis data acquisition, **Yong Wang**: NP's synthesis, and ligand transfer, **Ruiqi Yang**: NP's synthesis, and ligand transfer, **Katherine Leslee A. Cimatu**: Work supervision, **Olga Baturina**: Optical experiments with plasmonic strips, **Zhewei Wang**: Machine learning, and manuscript writing, **Jundong Liu**: Machine learning, and manuscript writing, **Joseph M. Slocik**: Conjugation protocol, and data discussion, **Shiyong Wu**: Work supervision, **Dongling Ma**: NPs synthesis, work supervision, data discussion, and manuscript writing, **Andrei I. Pastukhov**: NPs synthesis, **Andrei Kabashin**: NPs synthesis, work supervision, data discussion, and manuscript writing, **Martin E. Kordesch**: Imaging, work supervision, and data discussion, and **Alexander O. Govorov**: Conceptualization, manuscript writing, data discussion, and work supervision.

Interest declaration

None.

Additional Information

None.

ORCID

Verónica A. Bahamondes Lorca: 0000-0002-0488-2472

Óscar Ávalos-Ovando: 0000-0003-3572-7675

Christoph Sikeler:

Eva Yazmin Santiago: 0000-0001-8201-645X

Eli Skelton: 0000-0001-9441-5909

Yong Wang: 0000- 0001-8511-0097

Ruiqi Yang: 0009-0000-8677-9243

Katherine Leslee A. Cimatu: 0000-0002-4216-9715

Joseph M. Slocik: 0000-0001-5824-7709

Shiyong Wu: 0000-0002-4104-4160

Dongling Ma: 0000-0001-8558-3150

Andrei I. Pastukhov:

Andrei Kabashin: 0000-0003-1549-7198

Martin E. Kordesch: 0000-0001-7396-6525

Alexander O. Govorov: 0000-0003-1316-6758

References

1. Ferrari, E., *Gold Nanoparticle-Based Plasmonic Biosensors.* Biosensors (Basel), 2023. **13**(3).
2. Stater, E.P., A.Y. Sonay, C. Hart, and J. Grimm, *The ancillary effects of nanoparticles and their implications for nanomedicine.* Nat Nanotechnol, 2021. **16**(11): p. 1180-1194.
3. Altug, H., S.H. Oh, S.A. Maier, and J. Homola, *Advances and applications of nanophotonic biosensors.* Nat Nanotechnol, 2022. **17**(1): p. 5-16.
4. Kabashin, A.V., V.G. Kravets, and A.N. Grigorenko, *Label-free optical biosensing: going beyond the limits.* Chem Soc Rev, 2023. **52**(18): p. 6554-6585.
5. Wang, J., A.J. Drelich, C.M. Hopkins, S. Mecozzi, L. Li, G. Kwon, and S. Hong, *Gold nanoparticles in virus detection: Recent advances and potential considerations for SARS-CoV-2 testing development.* Wiley Interdiscip Rev Nanomed Nanobiotechnol, 2022. **14**(1): p. e1754.

6. Ardekani, L.S. and P.W. Thulstrup, *Gold Nanoparticle-Mediated Lateral Flow Assays for Detection of Host Antibodies and COVID-19 Proteins.* Nanomaterials (Basel), 2022. **12**(9).
7. Hwang, Y.C., R.M. Lu, S.C. Su, P.Y. Chiang, S.H. Ko, F.Y. Ke, K.H. Liang, T.Y. Hsieh, and H.C. Wu, *Monoclonal antibodies for COVID-19 therapy and SARS-CoV-2 detection.* J Biomed Sci, 2022. **29**(1): p. 1.
8. Chen, X., L. Ding, X. Huang, and Y. Xiong, *Tailoring noble metal nanoparticle designs to enable sensitive lateral flow immunoassay.* Theranostics, 2022. **12**(2): p. 574-602.
9. Koczula, K.M. and A. Gallotta, *Lateral flow assays.* Essays Biochem, 2016. **60**(1): p. 111-20.
10. Parolo, C., A. Sena-Torralba, J.F. Bergua, E. Calucho, C. Fuentes-Chust, L. Hu, L. Rivas, R. Alvarez-Diduk, E.P. Nguyen, S. Cinti, D. Quesada-Gonzalez, and A. Merkoci, *Tutorial: design and fabrication of nanoparticle-based lateral-flow immunoassays.* Nat Protoc, 2020. **15**(12): p. 3788-3816.
11. Gupta, R., P. Gupta, S. Wang, A. Melnykov, Q. Jiang, A. Seth, Z. Wang, J.J. Morrissey, I. George, S. Gandra, P. Sinha, G.A. Storch, B.A. Parikh, G.M. Genin, and S. Singamaneni, *Ultrasensitive lateral-flow assays via plasmonically active antibody-conjugated fluorescent nanoparticles.* Nat Biomed Eng, 2023. **7**: p. 1156-70.
12. Harper, J. *How Much Gold Is There Left to Mine in the World?* 2020; Available from: https://www.bbc.com/news/business-54230737.
13. ; Available from: https://www.researchandmarkets.com/report/metal-nanoparticles.
14. Jendrzej, S., B. Gokce, M. Epple, and S. Barcikowski, *How Size Determines the Value of Gold: Economic Aspects of Wet Chemical and Laser-Based Metal Colloid Synthesis.* Chemphyschem, 2017. **18**(9): p. 1012-1019.
15. Naik, G.V., V.M. Shalaev, and A. Boltasseva, *Alternative plasmonic materials: beyond gold and silver.* Adv Mater, 2013. **25**(24): p. 3264-94.
16. Wang, Y., Q. Zhang, Y. Wang, L.V. Besteiro, Y. Liu, H. Tan, Z.M. Wang, A.O. Govorov, J.Z. Zhang, J.K. Cooper, J. Zhao, G. Chen, M. Chaker, and D. Ma, *Ultrastable Plasmonic Cu-Based Core–Shell Nanoparticles.* Chemistry of Materials, 2020. **33**(2): p. 695-705.
17. Popov, A.A., G. Tselikov, N. Dumas, C. Berard, K. Metwally, N. Jones, A. Al-Kattan, B. Larrat, D. Braguer, S. Mensah, A. Da Silva, M.A. Esteve, and A.V. Kabashin, *Laser- synthesized TiN nanoparticles as promising plasmonic alternative for biomedical applications.* Sci Rep, 2019. **9**(1): p. 1194.
18. Zelepukin, I.V., A.A. Popov, V.O. Shipunova, G.V. Tikhonowski, A.B. Mirkasymov, E.A. Popova-Kuznetsova, S.M. Klimentov, A.V. Kabashin, and S.M. Deyev, *Laser-synthesized TiN nanoparticles for biomedical applications: Evaluation of safety, biodistribution and pharmacokinetics.* Mater Sci Eng C Mater Biol Appl, 2021. **120**: p. 111717.
19. Popov, A.A., G.V. Tikhonowski, P.V. Shakhov, E.A. Popova-Kuznetsova, G.I. Tselikov, R.I. Romanov, A.M. Markeev, S.M. Klimentov, and A.V. Kabashin, *Synthesis of Titanium Nitride Nanoparticles by Pulsed Laser Ablation in Different Aqueous and Organic Solutions.* Nanomaterials (Basel), 2022. **12**(10): p. 1672.
20. Rej, S., E.Y. Santiago, O. Baturina, Y. Zhang, S. Burger, S. Kment, A.O. Govorov, and A. Naldoni, *Colloidal titanium nitride nanobars for broadband inexpensive plasmonics and photochemistry from visible to mid-IR wavelengths.* Nano Energy, 2022. **104**: p. 107989.
21. Sultana, H., *Coupled Plasmon Wave Dynamics beyond Anomalous Reflection: A Phase Gradient Copper Metasurface for the Visible to Near-Infrared Spectrum.* Optics, 2022. **3**(3): p. 243-253.
22. Lalisse, A., G. Tessier, J. Plain, and G. Baffou, *Quantifying the Efficiency of Plasmonic Materials for Near-Field Enhancement and Photothermal Conversion.* The Journal of Physical Chemistry C, 2015. **119**(45): p. 25518-25528.

23. Das, A., A.C.M.V. Pereira, A.A. Popov, A. Pastukhov, S.M. Klimentov, A.V. Kabashin, and A.S.L. Gomes, *Plasmonically enhanced two-photon absorption induced photoacoustic microscopy with laser-synthesized TiN nanoparticles.* Applied Physics Letters, 2022. **121**(8): p. 83701.
24. Jiang, W., Q. Fu, H. Wei, and A. Yao, *TiN nanoparticles: synthesis and application as near-infrared photothermal agents for cancer therapy.* Journal of Materials Science, 2019. **54**(7): p. 5743-5756.
25. He, W., K. Ai, C. Jiang, Y. Li, X. Song, and L. Lu, *Plasmonic titanium nitride nanoparticles for in vivo photoacoustic tomography imaging and photothermal cancer therapy.* Biomaterials, 2017. **132**: p. 37-47.
26. Mi, X., H. Chen, J. Li, and H. Qiao, *Plasmonic Au-Cu nanostructures: Synthesis and applications.* Front Chem, 2023. **11**: p. 1153936.
27. Cao, W., T. Guo, J. Wang, G. Xu, J. Jiang, and D. Liu, *Cu-based materials: Design strategies (hollow, core-shell, and LDH), sensing performance optimization, and applications in small molecule detection.* Coordination Chemistry Reviews, 2023. **497**: p. 215450.
28. Farooq, S., C.V.P. Vital, G. Tikhonowski, A.A. Popov, S.M. Klimentov, L. A.G. Malagon, R.E. de Araujo, A.V. Kabashin, and D. Rativa, *Thermo-optical performance of bare laser-synthesized TiN nanofluids for direct absorption solar collector applications.* Solar Energy Materials and Solar Cells, 2023. **252**: p. 112203.
29. Rej, S., L. Mascaretti, E.Y. Santiago, O. Tomanec, Š. Kment, Z. Wang, R. Zbořil, P. Fornasiero, A.O. Govorov, and A. Naldoni, *Determining Plasmonic Hot Electrons and Photothermal Effects during H2 Evolution with TiN–Pt Nanohybrids.* ACS Catalysis, 2020. **10**(9): p. 5261-5271.
30. Chicco, D., *Siamese Neural Networks: An Overview.* Methods Mol Biol, 2021. **2190**: p. 73-94.
31. Gao, S., J.M. Guisan, and J. Rocha-Martin, *Oriented immobilization of antibodies onto sensing platforms - A critical review.* Anal Chim Acta, 2022. **1189**: p. 338907.
32. Mirica, A.C., D. Stan, I.C. Chelcea, C.M. Mihailescu, A. Ofiteru, and L.A. Bocancia-Mateescu, *Latest Trends in Lateral Flow Immunoassay (LFIA) Detection Labels and Conjugation Process.* Front Bioeng Biotechnol, 2022. **10**: p. 922772.
33. Ruiz, G., K. Tripathi, S. Okyem, and J.D. Driskell, *pH Impacts the Orientation of Antibody Adsorbed onto Gold Nanoparticles.* Bioconjug Chem, 2019. **30**(4): p. 1182-1191.
34. Zhou, S., J. Hu, X. Chen, H. Duan, Y. Shao, T. Lin, X. Li, X. Huang, and Y. Xiong, *Hydrazide-assisted directional antibody conjugation of gold nanoparticles to enhance immunochromatographic assay.* Anal Chim Acta, 2021. **1168**: p. 338623.
35. Hao, Y., Y. Li, L. Song, and Z. Deng, *Flash Synthesis of Spherical Nucleic Acids with Record DNA Density.* J Am Chem Soc, 2021. **143**(8): p. 3065-3069.
36. Lou, D., L. Fan, Y. Ji, N. Gu, and Y. Zhang, *A signal amplifying fluorescent nanoprobe and lateral flow assay for ultrasensitive detection of cardiac biomarker troponin I.* Analytical Methods, 2019. **11**(28): p. 3506-3513.
37. Lou, D., L. Fan, Y. Cui, Y. Zhu, N. Gu, and Y. Zhang, *Fluorescent Nanoprobes with Oriented Modified Antibodies to Improve Lateral Flow Immunoassay of Cardiac Troponin I.* Anal Chem, 2018. **90**(11): p. 6502-6508.
38. Lou, D., L. Ji, L. Fan, Y. Ji, N. Gu, and Y. Zhang, *Antibody-Oriented Strategy and Mechanism for the Preparation of Fluorescent Nanoprobes for Fast and Sensitive Immunodetection.* Langmuir, 2019. **35**(14): p. 4860-4867.
39. Grant, B.D., C.E. Anderson, J.R. Williford, L.F. Alonzo, V.A. Glukhova, D.S. Boyle, B.H. Weigl, and K.P. Nichols, *SARS-CoV-2 Coronavirus Nucleocapsid Antigen-Detecting Half-Strip Lateral Flow Assay Toward the Development of Point of Care Tests Using Commercially Available Reagents.* Anal Chem, 2020. **92**(16): p. 11305-11309.
40. Shrivastav, A.M., U. Cvelbar, and I. Abdulhalim, *A comprehensive review on plasmonic-based biosensors used in viral diagnostics.* Commun Biol, 2021. **4**(1): p. 70.

41. Baturina, O.A., A. Epshteyn, A.C. Leff, A.P. Purdy, T. Brintlinger, B.S. Simpkins, E.Y. Santiago, and A.O. Govorov, *Photoelectrochemical Methanol Oxidation Under Visible and UV Excitation of TiO2-Supported TiN and ZrN Plasmonic Nanoparticles.* Journal of The Electrochemical Society, 2021. **168**(1): p. 16503.
42. Johnson, P.B. and R.W. Christy, *Optical Constants of the Noble Metals.* Physical Review B, 1972. **6**(12): p. 4370-4379.
43. Guler, U., A.V. Kildishev, A. Boltasseva, and V.M. Shalaev, *Plasmonics on the slope of enlightenment: the role of transition metal nitrides.* Faraday Discuss, 2015. **178**: p. 71-86.
44. Siefke, T., S. Kroker, K. Pfeiffer, O. Puffky, K. Dietrich, D. Franta, I. Ohlídal, A. Szeghalmi, E.B. Kley, and A. Tünnermann, *Materials Pushing the Application Limits of Wire Grid Polarizers further into the Deep Ultraviolet Spectral Range.* Advanced Optical Materials, 2016. **4**(11): p. 1780-1786.

Supporting Information for

Lateral Flow Assays Biotesting by Utilizing Plasmonic Nanocrystals Made of Inexpensive Metals – Replacing Gold

Veronica A. Bahamondes Lorca[1,2], Oscar Ávalos-Ovando[3,4], Christoph Sikeler[5], Eva Yazmin Santiago[3,4], Eli Skelton[4,6], Yong Wang[7], Ruiqi Yang[7], Katherine Leslee A. Cimatu[4,6], Olga Baturina[8], Zhewei Wang[9], Jundong Liu[9], Joseph M. Slocik[10], Shiyong Wu[1,6], Dongling Ma[7], Andrei I. Pastukhov[11], Andrei Kabashin[11], Martin E. Kordesch[3,4], and Alexander O. Govorov[3,4*]

[1] Edison Biotechnology Institute, Ohio University, Athens, Ohio 45701, United States

[2] Departamento de Tecnología médica, Facultad de Medicina, Universidad de Chile, Santiago, Chile

[3] Department of Physics and Astronomy, Ohio University, Athens, Ohio 45701, United States

[4] Nanoscale and Quantum Phenomena Institute, Ohio University, Athens, Ohio 45701, United States

[5] Faculty of Physics and Center for NanoScience (CeNS), Ludwig Maximilians University, 80539 Munich, Germany

[6] Department of Chemistry and Biochemistry, Ohio University, Athens, Ohio 45701, United States

[7] Institut National de la Recherche Scientifique,Varennes, Québec J3X 1P7, Canada

[8] Chemistry Division, United States Naval Research Laboratory, Washington DC 20375, United States

[9] School of Electrical Engineering and Computer Science, Ohio University, Athens, Ohio 45701, United States

[10] Soft Matter Materials Branch, Materials and Manufacturing Directorate, Air Force Research Laboratory, Wright Patterson Air Force Base, Ohio 45433-7750, United States

[11] Laboratory LP3, Campus de Luminy, Aix-Marseille University, CNRS, 13288 Marseille, France

* Corresponding authors: govorov@ohio.edu

Keywords: optical activity, nanoparticles, lateral flow assay, biomarkers.

I. Theoretical Drude broadening model for TiN NPs.

Here we validate our particular choice of parameters for the core-shell model of TiN-TiO_2 NPs.

For the spherical Au NPs and Cu@Au NPs the numerical simulations of the extinction immediately fit the experimental absorption, as shown in Fig. 1B in the main text. This is done by using the experimentally measured dielectric constants available in the literature [1]; using the typical TEM characterized sizes 40 nm for Au NPs and 12 nm (11.5 nm of Cu and 0.5 nm of Au shell) for Cu@Au NPs; and following the formalism shown in the Materials and Methods section.

For the TiN NPs on the other hand, we need to account for oxidation and the inherent polydispersity inherited from the growth process [2]. This is found to be only achievable when a core-shell of TiN-TiO_2 is considered, accounting for slight oxidation of the outer NP shell. The TiN dielectric function is taken from Guler [3], and for TiO_2 from Siefke [4], and several combinations of values for the TiN-core and TiO_2-shell are tested. See Figure S1A for schematics. By simultaneously comparing with our experimental absorbance (red symbols). One can see that the total diameter of the NP does not play much role, but it just red-shifts the plasmon a few nanometers when simulating D=10 nm to D=40 nm (Figure S1B). The TiO_2 thickness on the other hand, does play a role by making the plasmon slightly wider and red-shifting it significantly, as shown in Figure S1C. Finally, these are the spectra (specifically, the one of 30 nm, 28 nm TiN and 2 nm of TiO_2 shell) we used in Figure 1B and for calculating the day-vision sensitivity efficiency parameter $V_{day-vision}(\lambda)$ of Figure 1C.

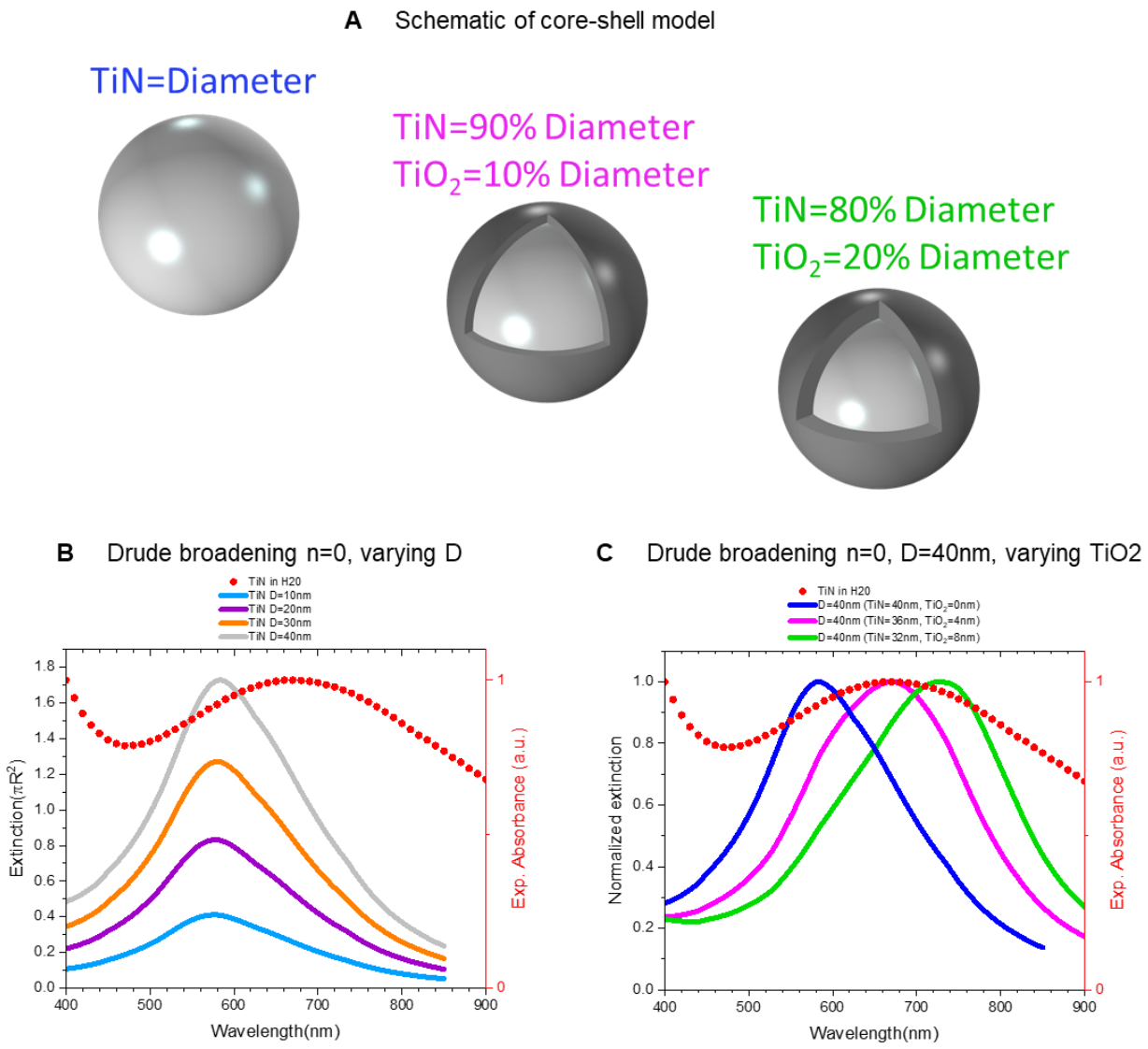

Figure S1. Models of TiN-TiO_2 core-shell and Drude broadening. A) Schematic representation of different aspect ratios between TiN-TiO_2 as shown. In all plots, lines are Comsol numerical simulations (left axis) and red symbols are our NPs experimental absorbance (right axis). B) Different diameters of TiN, no TiO_2. C) Same NPs diameters (D=40nm) with three TiN-TiO_2 aspect ratios.

II. Visible and Near-IR plasmonic characterization for the FITC study.

An important characteristic of these NPs is their plasmon, which should be preserved if the NPs want to be used in other approaches, as for example in the near-IR window above the day vision spectrum shown in Figure 1B. To confirm the plasmonic characteristics of the Cu@Au and TiN NPs are maintained after functionalization and LFA, we used the Odyssey XF Imager. This equipment has 3 channels, 685 nm, 785 nm, and 600 nm. Images of the LFAs were taken using each channel. If the NPs preserve their plasmonic characteristics, they will maintain the ability to absorb in the visible and near-IR ranges, and a dark line should be observed. As shown in Figure S2, the images of each channel show a dark line which correlates with the location and intensity of the control and testing line of the naked eye LFAs (showed in the main text on Figure 3C). Moreover, the intensity of the bands observed for each NPs in each channel, correlates with their plasmonic peak (Figure 3B), which confirms that the plasmonic characteristics of these NPs even after functionalization and attaching to the LFAs, is preserved.

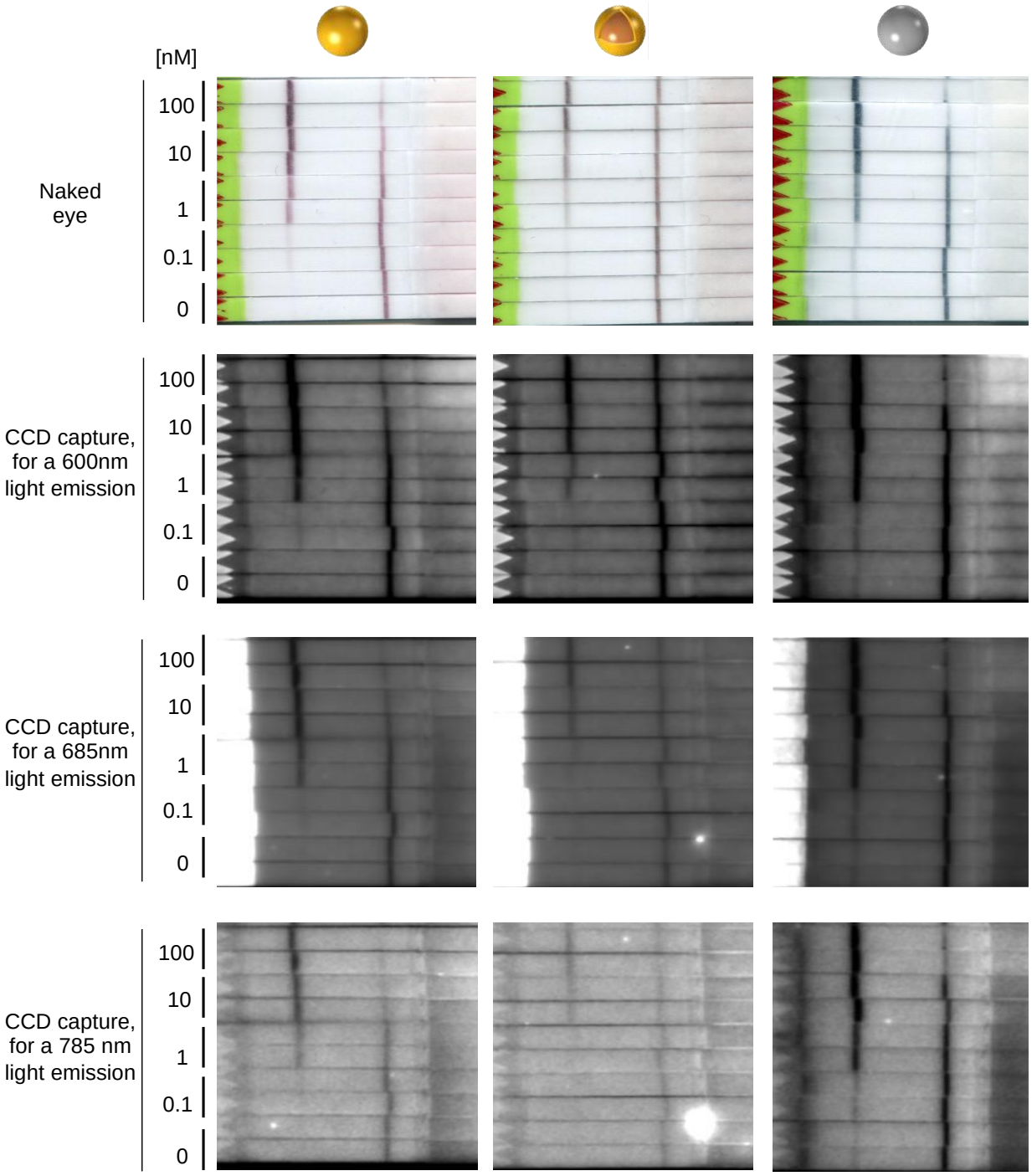

Figure S2. NPs preserve their plasmonic characteristics after functionalization and LFA. The LFAs on Figure 3C were imaged using the Odyssey XF Imager. *The LFAs images were taken using each channel (600 nm, 685 nm, and 785 nm) to analyze if the NPs preserved their plasmonic characteristics. As seen in these images, a dark line is observed in each LFAs, which correlated with the images obtained at naked eye. In addition, the images show that each NPs absorb different on each channel, which correlates with their absorption peak characterized in Figure 3B.*

III. NPs post-functionalization.

TEM imaging was developed to confirm that after functionalization the NPs are maintaining in suspension. We use both Cu@Au with the antibody anti-cTnT and TiNs with DNA as examples. The stability of the NPs in an aqueous medium after functionalization is of great importance for the future applicability of these NPs.

Figure S3A was obtained as indicated in the main text, in the materials and methods section. In Figure S3B, the TiN NPs were functionalized using a different approach, to demonstrate the flexibility of conjugation these NPs have. TiN NPs shown in Figure S3B were functionalized with DNA, composed of a thiol group at the 5' end of 19 consecutive thymine bases, ordered from biomers, that will react with the titanium forming a titanium sulfide bridge between the TiN NPs and the DNA. The method for functionalization was instant dehydration in butanol [5]. Figure S3B shows that even with this different protocol of functionalization, the TiN NPs do not aggregate. The images were taken using the TEM JEM-1011 transmission electron microscope from JEOL.

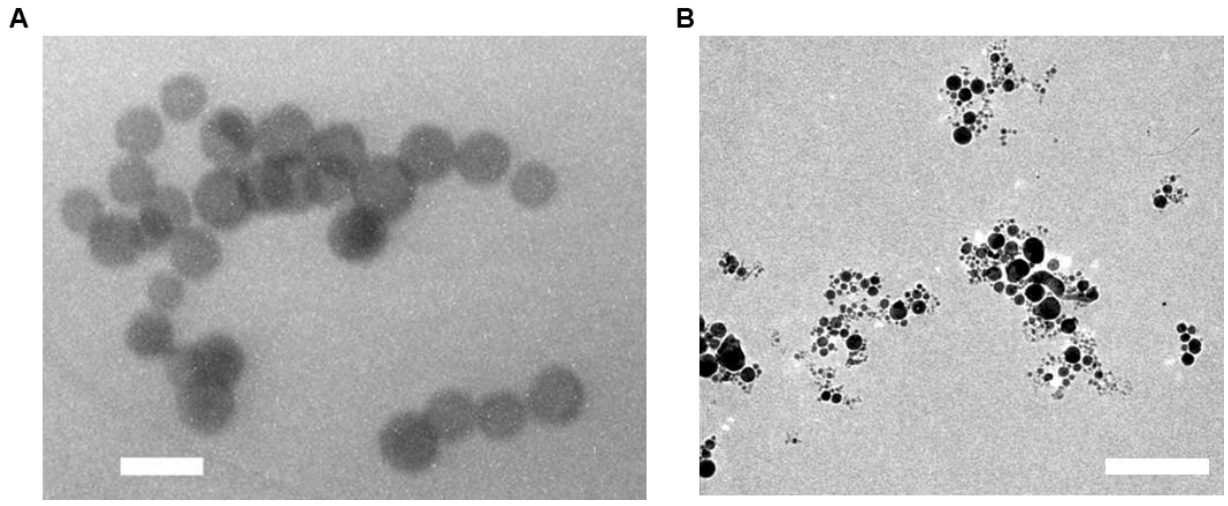

Figure S3. TEM images of NPs after functionalization. A) TEM image of the Cu@Au NPs conjugated with the antibody anti-cTnT (bar 20 nm). B) TEM image of the TiN NPs functionalized with DNA (bar 200 nm). This image demonstrates that different approaches can be used for successfully conjugating the NPs. In this case, DNA composed of 19 thymine based was utilized.

IV. Plasmon shift for anti-cTnT functionalization.

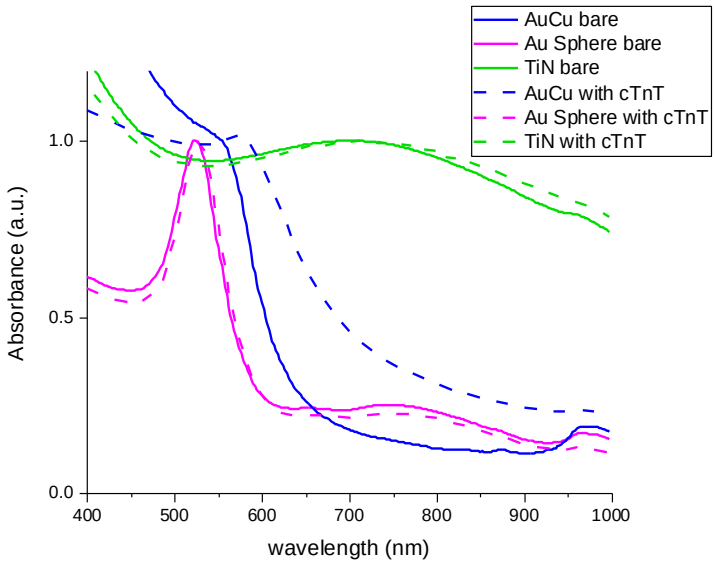

	bare	Conjugated
Au spheres	524 nm	528 nm
TiN	694 nm	708 nm
AuCu	554 nm	570 nm

Figure S4. Absorbance of the Cu@Au and TiN NPs pre and post anti-cTnT conjugation. Here, we can see the plot and a table comparing the plasmons for each NPs before (solid lines) and after (dashed lines) conjugation with the anti-cTnT antibody. The results support the successful functionalization of each NPs with the antibody.

V. References for supporting information.

1. Johnson, P.B. and R.W. Christy, *Optical Constants of the Noble Metals.* Physical Review B, 1972. **6**(12): p. 4370-4379.
2. Baturina, O.A., et al., *Photoelectrochemical Methanol Oxidation Under Visible and UV Excitation of TiO2-Supported TiN and ZrN Plasmonic Nanoparticles.* Journal of The Electrochemical Society, 2021. **168**(1).
3. Guler, U., et al., *Plasmonics on the slope of enlightenment: the role of transition metal nitrides.* Faraday Discuss, 2015. **178**: p. 71-86.
4. Siefke, T., et al., *Materials Pushing the Application Limits of Wire Grid Polarizers further into the Deep Ultraviolet Spectral Range.* Advanced Optical Materials, 2016. **4**(11): p. 1780-1786.
5. Hao, Y., et al., *Flash Synthesis of Spherical Nucleic Acids with Record DNA Density.* J Am Chem Soc, 2021. **143**(8): p. 3065-3069.